Highly Porous Cellulose-Based Carbon Fibers as Effective Adsorbents for Chlorpyrifos Removal: Insights and Applications

Tamara Tasić [1], Vedran Milanković [1], Christoph Unterweger [2], Christian Fürst [2], Stefan Breitenbach [2,3], Igor A. Pašti [4] and Tamara Lazarević-Pašti [1,*]

[1] VINCA Institute of Nuclear Sciences—National Institute of the Republic of Serbia, University of Belgrade, Mike Petrovica Alasa 12–14, 11000 Belgrade, Serbia; tamara.tasic@vin.bg.ac.rs (T.T.); vedran.milankovic@vin.bg.ac.rs (V.M.)

[2] Wood K Plus—Kompetenzzentrum Holz GmbH, Altenberger Strasse 69, 4040 Linz, Austria; c.unterweger@wood-kplus.at (C.U.); c.fuerst@wood-kplus.at (C.F.); s.breitenbach@wood-kplus.at (S.B.)

[3] Institute of Chemical Technology of Inorganic Materials (TIM), Johannes Kepler University Linz, Altenberger Strasse 69, 4040 Linz, Austria

[4] Faculty of Physical Chemistry, University of Belgrade, Studentski Trg 12-16, 11158 Belgrade, Serbia; igor@ffh.bg.ac.rs

[*] Correspondence: tamara@vin.bg.ac.rs

Abstract: The extensive utilization of the organophosphate pesticide chlorpyrifos, combined with its acute neurotoxicity, necessitates the development of effective strategies for its environmental removal. While numerous methods have been explored for chlorpyrifos removal from water, adsorption is the most promising. We investigated the potential of two cellulose-derived porous carbons as adsorbents for chlorpyrifos removal from water, prepared by either CO_2 or H_2O activation, resulting in similar morphologies and porosities but different amounts of heteroatom functionalities. The kinetics of batch adsorption removal from water fits well with the pseudo-first-order and pseudo-second-order kinetic models for both materials. The Freundlich, Langmuir, Dubinin–Radushkevich, and Sips isotherm models described the process of chlorpyrifos adsorption very well in all investigated cases. The maximum adsorption capacity determined from the Sips isotherm model gave values of 80.8 ± 0.1 mg g^{-1} and 132 ± 3 mg g^{-1} for the H_2O and CO_2 activated samples, respectively, reflecting the samples' differences in heteroatom functionalities. Additionally, the application of either adsorbent led to reduced toxicity levels in all tested samples, implying that no harmful by-products were generated during adsorption. Comparative analysis with the existing literature further validates the study's findings, suggesting the efficacy and applicability of cellulose-based porous carbons for sustainable chlorpyrifos remediation.

Keywords: organophosphate; pesticide remediation; cellulose; adsorption; neurotoxicity

1. Introduction

Chlorpyrifos (CHP) is a widely used organophosphate pesticide in agriculture and is well known for its effectiveness against a broad spectrum of pests [1]. Its significance stems from several key factors. Firstly, CHP is valued for its efficacy in controlling various agricultural pests, including aphids, caterpillars, beetles, and mites, making it a versatile tool for farmers across various crops [2]. Moreover, its ability to persist on treated crops and soil provides prolonged protection against pests, particularly in regions with continuous pest pressure throughout the growing season [3]. Additionally, CHP is considered cost-effective compared to other alternatives, making it an attractive choice for farmers, especially in pest-prone areas. Its versatility in various formulations like liquids, granules, and dusts allows for flexible application methods tailored to different crop types, pest species, and environmental conditions [4]. Furthermore, with a history dating back to the 1960s [5],

CHP has earned farmers' trust due to its reliability and proven effectiveness over decades, solidifying its widespread adoption in agriculture as a go-to pesticide for protecting crops.

However, it was proven that CHP poses significant environmental and health concerns due to its persistence and potential toxicity to non-target organisms, including humans [6,7]. Its extended persistence in the environment increases the risk of chronic exposure to both target and non-target organisms, with residues leaching into groundwater and contaminating aquatic ecosystems [8]. Acute exposure to CHP can result in symptoms ranging from nausea and dizziness to convulsions or death [9,10], while chronic low-level exposure, especially during critical developmental stages, has been associated with neurological developmental delays and cognitive deficits in children [11,12]. Additionally, CHP's non-selective toxicity poses risks to beneficial insects [13,14], birds [13,14], and aquatic life [14,15], disrupting ecological balance and agricultural productivity.

Adsorption is a crucial and efficient remediation strategy for mitigating CHP contamination in soil and water environments due to its effectiveness, simplicity, and environmental compatibility [16,17]. By utilizing adsorbent materials, such as carbon-based substances, CHP molecules can be selectively captured and immobilized onto the surface of the adsorbent, effectively removing them from the contaminated media. This process achieves high removal efficiencies and reduces CHP concentrations to safe levels, minimizing the risks associated with CHP exposure to human health and the environment [16,17]. Adsorption offers several advantages, including cost-effectiveness, minimal energy requirements, and optimizing adsorption capacities by manipulating material properties [18].

Carbon-based porous materials offer several advantages for adsorption applications, making them highly effective at removing contaminants like CHP from soil and water environments. Firstly, carbon-based materials can possess exceptionally high surface areas due to their porous structures, providing plenty of adsorption sites for molecules' adsorption. This increased surface area enhances the adsorption capacity of the material, allowing for the efficient removal of contaminants [19,20]. Additionally, the porous structure of carbon-based materials facilitates rapid diffusion of contaminants into the material's interior, further enhancing adsorption efficiency [19]. Moreover, the surface chemistry of carbon-based materials can be easily modified or tailored to enhance adsorption selectivity towards specific contaminants. This tunable surface chemistry optimizes adsorption properties, making carbon-based porous materials versatile and adaptable for various adsorption applications [21].

Cellulose-derived porous carbons represent a promising class of carbon-based materials with diverse applications in various fields, including environmental remediation, energy storage, and catalysis [22,23]. The synthesis of cellulose-derived porous carbons typically involves a multi-step process, beginning with the dissolution of cellulose from natural sources in a suitable solvent, followed by spinning or casting to form precursor fibers or films. Subsequent thermal treatment, such as carbonization and activation, transforms the precursor materials into carbonaceous structures while removing volatile components, forming porous carbon materials [17,22]. Additionally, cellulose is easily chemically modifiable, enhancing its versatility for specific uses and enabling the preparation of diverse macroporous structures like textiles, papers, or aerogels [24–26]. The usually small and constant diameter of cellulose fibers allows narrow pore size distributions to be achieved in contrast to granular precursor materials. Due to their small dimensions, activated carbon fibers have pores mostly situated at the fiber surface and thus provide good accessibility to their active sites [27]. In our previous study, we showed that cellulose-based activated carbon fibers contain pores in the micropore and mesopore ranges [22]. In combination with the above-mentioned macroporous structures or macropores being formed between the single fibers, cellulose-derived porous carbons can exhibit a hierarchical porous structure comprising micropores, mesopores, and macropores, which has been described as advantageous for various applications, including enhanced adsorption capacities [28,29]. These materials' specific surface area and pore size distribution can be tailored through control over precursor composition, processing conditions, and activation methods. Ad-

ditionally, the surface chemistry of cellulose-derived carbon materials can be modified through functionalization or doping with heteroatoms, further enhancing their adsorption selectivity and catalytic properties [16,17].

In environmental remediation, these materials demonstrate excellent adsorption capabilities for various pollutants, including organic contaminants, heavy metals, and emerging contaminants like CHP. Moreover, their high surface area and porous structure enable the efficient capture and removal of contaminants from water and soil matrices [22].

The existing literature on the adsorption of CHP onto carbon-based materials reveals a significant research gap concerning the limited exploration of biomass-derived carbon materials in this context. While numerous studies have investigated the adsorption behavior of CHP on various carbonaceous substrates, including activated carbons, carbon nanotubes, and graphene-based materials, there is a notable insufficiency of research specifically focusing on biomass-derived carbon materials. This research gap is particularly noteworthy given the unique properties of cellulose-derived porous carbons, as already mentioned above, which offer potential advantages for CHP adsorption applications. The limited exploration of cellulose-derived carbon materials in CHP adsorption studies represents an untapped opportunity to advance our understanding of their adsorption mechanisms, optimize their adsorption capacities, and expand their practical applications in environmental remediation.

This study investigates the potential of using cellulose-derived porous carbons as an adsorbent for CHP removal from water. Initially, the manuscript presents the results of the physicochemical characterization of these materials. Following this, CHP adsorption onto cellulose-based carbon materials in water is conducted. The kinetics and thermodynamics of CHP adsorption on these materials are thoroughly investigated and discussed. Furthermore, the neurotoxicity of the water samples is closely monitored throughout the remediation process, aiming to identify the potential formation of more toxic by-products, such as oxo-forms of pesticides. Finally, the results obtained from this study were compared with those from the literature to assess their comparability.

2. Materials and Methods

2.1. Adsorbent Preparation and Characterization

In order to prepare adsorbents, cellulose fibers (Viscose 1.7 dtex, 38 mm, Lenzing AG, Lenzing, Austria) were impregnated in a 7.4 wt% diammonium hydrogen phosphate (DAHP) solution and carbonized in a nitrogen atmosphere at a heating rate of $1\,^\circ\text{C min}^{-1}$ until 850 °C followed by an isothermal step for 30 min. The subsequent activation was performed with a carbon dioxide flow of $80\,\text{L h}^{-1}$ (adsorbent VF_{CO_2}) or water vapor (adsorbent $\text{VF}_{\text{H}_2\text{O}}$), enabled by the injection of water ($1.0\,\text{mL min}^{-1}$) with a peristaltic pump. In both cases, the activation was performed at 870 °C for 165 min.

The examination of samples' structure and elemental composition utilized the Phenom-ProX Scanning Electron Microscope (SEM) provided by Thermo Fisher Scientific (Waltham, MA, USA) combined with Energy Dispersive X-ray Analysis (EDX).

N_2 adsorption at an isothermal temperature of $-196.15\,^\circ\text{C}$ was used in a gas sorption system (Autosorb-iQ, Anton Paar QuantaTec Inc., Graz, Austria) to examine the specific surface area and total pore volume of the samples. The samples were outgassed for 2 h at 200 °C under vacuum before analysis.

2.2. Adsorption Experiments

The adsorption experiments were conducted under batch (stationary) conditions. Initially, the adsorbents were dispersed in double-distilled water. To achieve the desired concentration of both the adsorbent and CHP, an appropriate amount of the organophosphate stock solution (Pestanal, Sigma Aldrich, Søborg, Denmark) was added. The mixture of adsorbent and CHP underwent shaking and incubation at 25 °C for specified durations using a laboratory shaker (Orbital Shaker-Incubator ES-20, Grant-Bio, Cambridgeshire, UK). Following incubation, the mixture underwent centrifugation at 14,500 rpm for 10 min. Su-

pernatant filtration was performed using a nylon filter (pore size 220 nm KX Syringe Filter, Kinesis, Cole Parmer, St. Neots, UK). The resulting filtrate underwent ultra-performance liquid chromatography (UPLC) analysis to determine the concentration of organophosphates after adsorption.

The adsorption efficiency, denoted as uptake, was calculated using the following formula: uptake = $100\% \times (C_0 - C_{eq})/C_0$, where C_0 represents the initial concentration of organophosphates. The concentrations of CHP in filtrates after adsorption (C_{eq}) were determined using UPLC. Control experiments were conducted under the same conditions as batch experiments but without the presence of adsorbents.

CHP analysis was conducted using the Waters ACQUITY UPLC system with a photodiode array (PDA) detector controlled by the Empower 3 version software. The ACQUITY UPLC™ BEH C18 column (1.7 μm, 100 mm × 2.1 mm, Waters GmbH, Eschborn, Germany) was utilized under isocratic conditions, with 10% acetonitrile in water (*v/v*) as mobile phase A and pure acetonitrile as mobile phase B. The eluent flow rate was 0.25 mL min^{-1}, and the injection volume was consistent at 5 μL. The analysis employed a mobile phase composition of 20% A and 80% B. The retention time was (2.70 ± 0.05) min, and it was detected at 205 nm.

2.3. Neurotoxicity of Chlorpyrifos

The neurotoxicity of CHP solutions was evaluated through measurements of AChE inhibition, aiming to track and quantify changes in toxicity before and after adsorption. This approach also enabled an investigation into potential transformations of CHP into more toxic forms during hydrolysis or oxidation, which could exert harmful effects at concentrations below the detection limits of UPLC. A modified Ellman's procedure [30,31] was employed to assay AChE activity, with in vitro experiments conducted by exposing 1 U/mL AChE to CHP solutions pre- and post-adsorption at 37 °C in 50 mmol dm^{-3} phosphate buffer at pH 8.0 (final volume 0.650 cm^3). The enzymatic reaction was initiated by adding acetylcholine-iodide along with 5,5′-dithio-bis-(2-nitrobenzoic acid) (DTNB) as a chromogenic reagent and allowed to proceed for 8 min before being halted by 10% sodium dodecyl sulfate (SDS). The resultant enzymatic reaction product, thiocholine, reacted with DTNB to form 5-thio-2-nitrobenzoate, whose optical absorption was measured at 412 nm. Physiological effects were quantified as AChE inhibition, expressed as a percentage according to the formula: AChE inhibition (%) = $100 \times (A_0 - A)/A_0$, where A_0 represents the AChE activity in the absence of CHP and A represents the activity measured after exposure to CHP. Acetylcholinesterase from electric eel, acetylthiocholine iodide (ASChI), and DTNB were procured from Sigma-Aldrich St. Louis, MO, USA, while potassium-hydrogen phosphate ($K_2HPO_4 \cdot 3H_2O$) and acetonitrile were obtained from Merck KgaA, Darmstadt, Germany.

3. Results and Discussion

3.1. SEM and EDX of the Synthesized Adsorbents

SEM was utilized to assess the morphology of the samples, with SEM micrographs of samples VF_{H_2O} and VF_{CO_2} presented in Figure 1(a1–a4). The micrographs show that the morphology of these samples remains consistent and reflects that of the precursor cellulose fibers (besides shrinkage of approx. 30%). This observation aligns with our previous research findings [17,22,32]. Additionally, the chemical composition of the investigated activated carbon fibers was analyzed using EDX (see mapping in Figure 1(b1–b5)). For both materials, carbon was identified as the dominant element in all samples with 91.3% and 84.7%, followed by oxygen with 8.5% and 13.6% and phosphorus with 0% and 1.6%, for VF_{H_2O} and VF_{CO_2}, respectively. The phosphorus found in the VF_{CO_2} sample originates from the impregnation with DAHP, and it was effectively removed by H_2O steam as well as a significant amount of surface oxygen, suggesting that P is in the form of phosphates on the VF surface. Minor traces of sodium at 0.13% and 0.11% and sulfur at 0.04% and 0% were also found in VF_{H_2O} and VF_{CO_2}, in that order, likely originating from the precursor

material. The distributions of the elements found in the samples were found to be uniform, without apparent separation of phases with higher concentrations of particular elements.
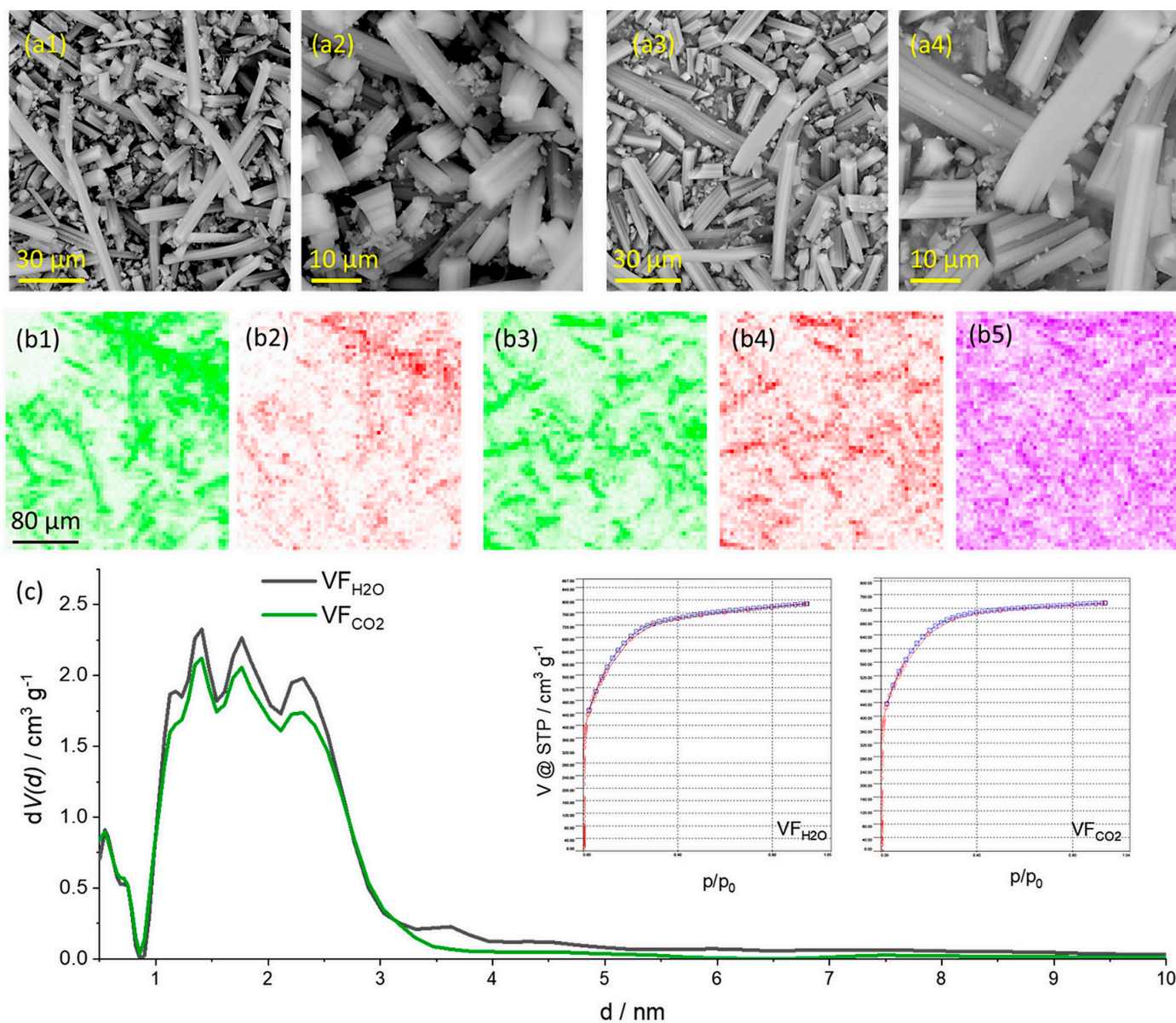

Figure 1. SEM micrographs of VF_{H2O} (**a1**,**a2**) and VF_{CO2} (**a3**,**a4**) at magnification ×2000 and ×5000. The middle row shows EDX maps of VF_{H2O} (**b1**—carbon; **b2**—oxygen) and VF_{CO2} (**b3**—carbon; **b4**—oxygen; **b5**—phosphorus), bottom row (**c**) shows pore size distributions of the two samples, with insets giving adsorption/desorption isotherms.

Considering the specific surface areas and pore volumes of the studied samples, there is another observation that is very important for the analysis of materials' performance as adsorbents. Namely, the specific surfaces (S_{BET}) are very similar and amount to 2443 m^2 g^{-1} for the VF_{H2O} sample and 2323 m^2 g^{-1} for the VF_{CO2} sample. The difference is only 5%, which is close to the uncertainty of the applied BET method, suggesting that the surface areas of these two samples are practically the same. The identical situation is found for total pore volumes (V_{tot}), where we found a V_{tot} of 1.22 cm^3 g^{-1} and 1.14 cm^3 g^{-1} for VF_{H2O} and VF_{CO_2}, respectively, i.e., a 6.6% difference. This small difference is visible in the pore size distribution (PSD) curves (Figure 1c), but overall, the distributions are very similar.

3.2. Adsorption Kinetics

The kinetics of CHP adsorption onto VF_{H_2O} and VF_{CO_2} were examined utilizing various models, including the non-linear pseudo-first (PFO) and pseudo-second-order (PSO) models, the Elovich kinetic model, and the intraparticle diffusion model. These models' formulations are detailed in Table 1 as follows:

Table 1. Equations for kinetic models.

Kinetic Model	Equation
Pseudo-first-order model	$q_t = q_e \left(1 - e^{-k_1 t} \right)$
Pseudo-second-order model	$q_t = \frac{q_e^2 k_2 t}{1 + q_e k_2 t}$
Elovich kinetic model	$q_t = \frac{1}{\beta}(1 + \alpha \beta t)$
Intraparticle diffusion model	$q_t = k_{id} t^{0.5} + C$

In these equations, q_t denotes the quantity of adsorbed adsorbate at time t (mg g^{-1}), while q_e signifies the equilibrium adsorption capacity (mg g^{-1}). The rate constants k_1 (min^{-1}) and k_2 (g mg^{-1} min^{-1}) describe the adsorption rate for the PFO and PSO models. Within the Elovich model, α denotes the initial adsorption rate (mg g^{-1} min^{-1}), and β represents the desorption constant (g mg^{-1}). The parameter k_{id} in the intraparticle diffusion model characterizes the adsorption rate constant (mg g^{-1} min$^{-0.5}$), while C denotes the boundary layer (mg g^{-1}).

The experimental data, alongside their corresponding fits, are presented in Figures 2 and 3. The derived equilibrium adsorption capacities and rate constants are tabulated in Tables 2 and 3, respectively.
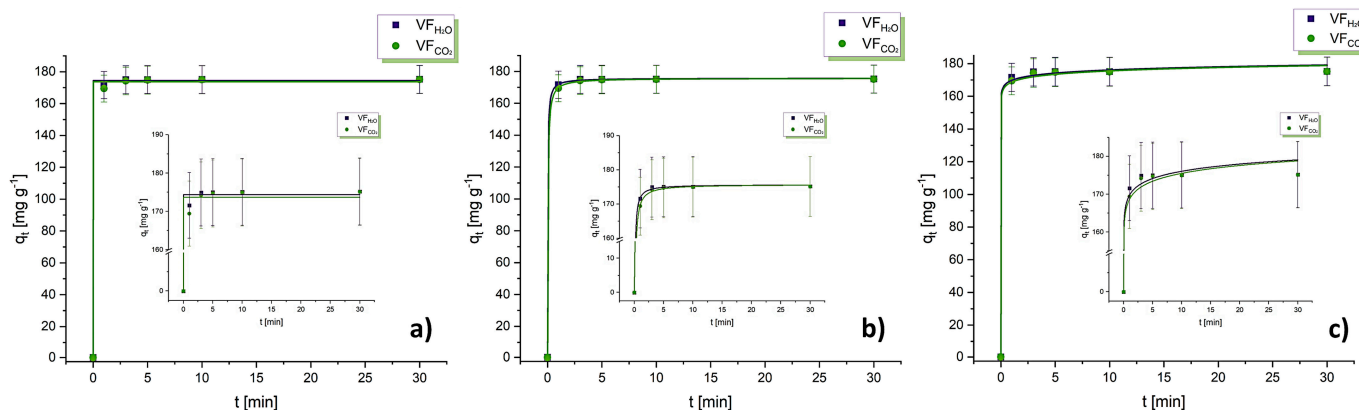

Figure 2. Graphical representation of kinetic models for CHP adsorption (concentration 5×10^{-4} mol dm^{-3}) onto carbon materials VF_{H_2O} and VF_{CO2} (concentration 1 mg mL^{-1}) at 25 °C using non-linear (**a**) PFO, (**b**) PSO, and (**c**) Elovich model.

From Figure 2, it can be seen that the adsorption equilibrium for removing CHP is achieved in 10 min, indicating rapid adsorption of CHP on both materials. Also, the experimental data aligned very well with the PSO and PFO models, as indicated by the high R^2 and low χ^2 values. The q_e values from both kinetic models are similar, confirming both fit robustness. It can be unambiguously concluded that the adsorption of CHP onto VF_{CO2} materials is slower compared to the VF_{H2O} material, according to k_1 and k_2 values and their corresponding uncertainties. By observing α values obtained from the Elovich kinetic model, which are very high, and β, which are very low, it can be concluded that the initial CHP adsorption rate onto the investigated materials is very high. These results confirmed previous statements regarding PFO and PSO.
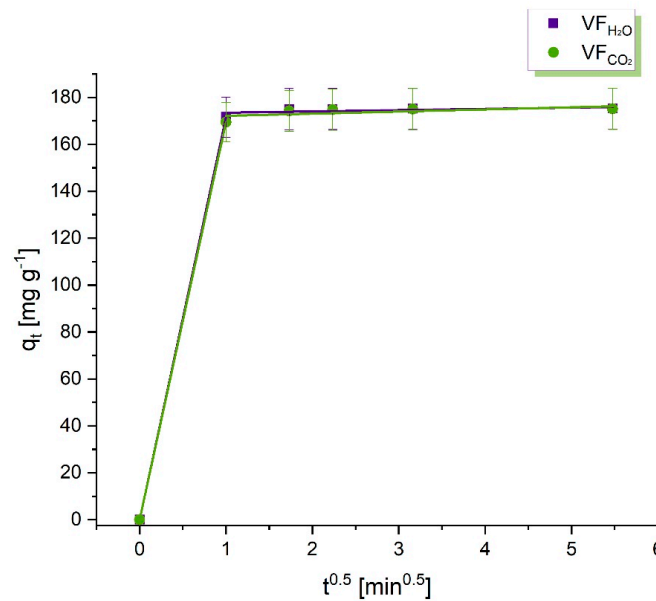
Figure 3. Intraparticle diffusion model for CHP adsorption (concentration 5×10^{-4} mol dm^{-3}) onto carbon materials VF$_{H2O}$ and VF$_{CO2}$ (concentration 1 mg mL^{-1}).

Table 2. Kinetic parameters for CHP adsorption (concentration 5×10^{-4} mol dm^{-3}) onto carbon materials VF$_{H2O}$ and VF$_{CO2}$ (concentration 1 mg mL^{-1}) at 25 °C.

Material	Pseudo-First-Order Kinetics			
	q_e (mg g^{-1})	k_1 (min^{-1})	χ^2	R^2
VF$_{H2O}$	174 ± 1	$(5.71 \pm 0.01) \times 10^4$	2.443	0.999
VF$_{CO2}$	174 ± 1	$(4.99 \pm 0.01) \times 10^4$	5.799	0.999
	Pseudo-second-order kinetics			
	q_e (mg g^{-1})	k_2 (min^{-1})	χ^2	R^2
VF$_{H2O}$	176 ± 1	0.251 ± 0.001	0.147	0.999
VF$_{CO2}$	176 ± 1	0.158 ± 0.001	0.150	0.999
	Elovich model			
	α (mg g^{-1} min^{-1})	β (g mg^{-1})	χ^2	R^2
VF$_{H2O}$	$(1.74 \pm 0.01) \times 10^{27}$	0.364 ± 0.001	6.317	0.999
VF$_{CO2}$	$(8.93 \pm 0.01) \times 10^{24}$	0.334 ± 0.001	5.366	0.999

Table 3. Kinetic parameters for intraparticle diffusion model of CHP (concentration 5×10^{-4} mol dm^{-3}) adsorption onto investigated adsorbents (concentration 1 mg mL^{-1}).

Material		Intraparticle Diffusion Model	
VF$_{H2O}$	I part	C (mg g^{-1})	0
		k_{id} (mg g^{-1} min$^{-0.5}$)	172 ± 1
	II part	C (mg g^{-1})	173 ± 4
		k_{id} (mg g^{-1} min$^{-0.5}$)	0.539 ± 0.006
VF$_{CO2}$	I part	C (mg g^{-1})	0
		k_{id} (mg g^{-1} min$^{-0.5}$)	169 ± 1
	II part	C (mg g^{-1})	171 ± 3
		k_{id} (mg g^{-1} min$^{-0.5}$)	0.904 ± 0.009

The intraparticle diffusion model showed two linear stages for CHP adsorption onto both materials. The first stage characterizes the diffusion of CHP molecules from the

solution to the external surface of materials. In contrast, the second stage is associated with the final equilibrium stage. The k_{id} values decrease after the breakpoints, indicating a slower adsorption rate in each consecutive stage. The boundary layer increases throughout stages, reaching values comparable with q_e values obtained from PFO and PSO models. It suggests that the boundary layer in CHP's adsorption process onto materials is highly significant.

However, we should note that the kinetic analysis is performed using the data that point to an extremely fast reaching of the adsorption equilibrium, while the main information about the kinetics of adsorption is stored in the initial part of the q_t vs. t curve, which is largely inaccessible to accurate measurements due to technical limitations. For these reasons, we do not unambiguously ascribe the adsorption process to any of the applied kinetic models and note that the absolute values of kinetic parameters should be taken with care. On the other hand, it is safe to conclude that the adsorption process is indeed faster on the VF_{H2O} sample, which is also obvious from the measured data points.

3.3. Adsorption Isotherms

Adsorption isotherms describe the process of CHP adsorption onto synthesized carbon materials and enable obtaining information about the adsorption mechanism, as well as the surface characteristics and affinities of the investigated materials towards the investigated pesticide. Experimental data were analyzed using the non-linear Freundlich, Langmuir, Temkin, Dubinin–Radushkevich, and Sips adsorption isotherms. Their equations are presented in the following Table 4, where q_e (mg g^{-1}) represents equilibrium adsorption capacity, C_e (mg dm^{-3}) equilibrium adsorbate concentration, K_F ((dm^3 mg^{-1})$^{1/n}$) and n as Freundlich constants, K_L (dm^3 mg^{-1}) and q_{max} (mg g^{-1}) as Langmuir constant and theoretical maximum adsorption capacity of the monolayer, b_T (J g mol^{-1} mg^{-1}) and K_T (dm^3 mg^{-1}) for Temkin isotherm constants, q_{DR} for maximum adsorption capacity, K_{DR} (mol^2 J^{-2}) for the constant associated with the mean free adsorption energy per mole of adsorbent ($\varepsilon = RT \times \ln(1 + 1/C_e)$), K_s (dm^3 mg^{-1}) and b_s represent Sips isotherm constants.

Table 4. Adsorption isotherm models' equations.

Adsorption Isotherm Model	Equation
Freundlich model	$q_e = K_F C_e^{\frac{1}{n}}$
Langmuir model	$q_e = \frac{q_{max} K_L C_e}{1 + K_L C_e}$
Temkin model	$q_e = \frac{RT}{b_T} \ln K_T C_e$
Dubinin–Radushkevic model	$q_e = q_{DR} e^{-K_{DR} \varepsilon^2}$
Sips model	$q_e = \frac{q_{max}(K_s C_e)^{b_s}}{1 + (K_s C_e)^{b_s}}$

The obtained isotherms are depicted in Figure 4, and the parameters of the adsorption isotherms are shown in Table 5. Figure 4 illustrates the non-linear fitting forms of all investigated isotherms for CHP adsorption onto VF_{H_2O} and VF_{CO_2} materials. Based on the parameters presented in Table 5, all applied models fit reasonably well with the experimental results, but the Freundlich, Langmuir, Dubinin–Radushkevich, and Sips isotherm models best described the experimental data, while the Temkin isotherm gave relatively large χ^2 values. As already known, the Sips isotherm combines Langmuir and Freundlich isotherm models [33,34]. It is a more flexible model for describing adsorption in systems exhibiting monolayer and multilayer adsorption. Also, it introduces an additional parameter known as the heterogeneity factor (denoted as b_s), which enables a smoother transition between Langmuir and Freundlich behaviors. The Sips isotherm yields better results in describing experimental data compared to the standalone use of Langmuir or Freundlich isotherms, particularly in cases where the adsorption behavior deviates from ideal monolayer or multilayer adsorption, which is not surprising in the case of heterogeneous surfaces with different possible adsorption sites or adsorption domains.
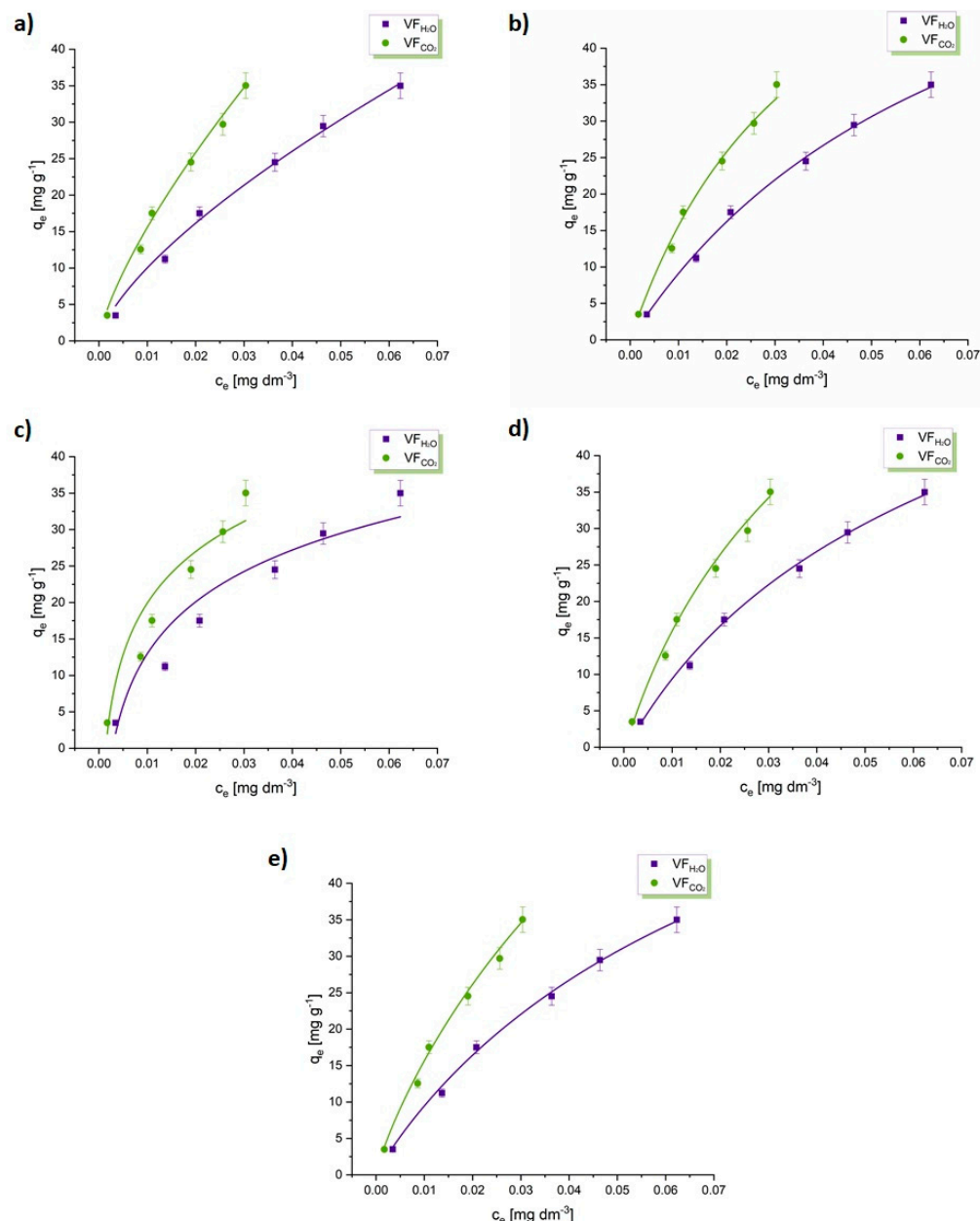
Figure 4. Non-linear adsorption isotherm models for CHP: (**a**) Freundlich, (**b**) Langmuir, (**c**) Temkin, (**d**) Dubinin–Raduskevic, and (**e**) Sips model, adsorbent dose 1 mg mL^{-1} at 25 °C.

The n value of the Freundlich isotherm model is higher than 1, indicating that adsorption is a favorable process. From the Langmuir model, we can see that the adsorption capacities of CHP are 73 mg g^{-1} and 75 mg g^{-1}. However, when observing the q_{max} values from the Sips isotherm, we can see that they are 80.8 ± 0.1 mg g^{-1} and 132 ± 3 mg g^{-1} for VF_{H2O} and VF_{CO2}, respectively, indicating that these investigated materials have a high potential to adsorb CHP. A similar conclusion can be derived from the results of the DR model fit, where q_{DR} was found to be 76.4 ± 0.1 and 101 ± 2 mg g^{-1} for VF_{H2O} and VF_{CO2}, respectively.

Given that the values for the parameter b_s are less than 1 for both materials and considering all the above-mentioned information, we can conclude that the adsorption process is most likely multilayer adsorption on the heterogeneous surface of carbon materials [35,36].

Table 5. Parameters for CHP adsorption using Freundlich, Langmuir, Temkin, Dubinin–Raduskevich, and Sips adsorption isotherm, adsorbent dose 1 mg mL^{-1}.

Material	Freundlich Isotherm			
	K_F ((dm^3 mg^{-1})$^{1/n}$)	n	χ^2	R^2
VF$_{H2O}$	239 ± 2	1.45 ± 0.04	1.341	0.992
VF$_{CO2}$	451 ± 1	1.37 ± 0.02	0.778	0.996
	Langmuir Isotherm			
	K_L (dm^3 mg^{-1})	q_{max} (mg g^{-1})	χ^2	R^2
VF$_{H2O}$	26.91 ± 0.4	73 ± 6	2.101	0.993
VF$_{CO2}$	13.77 ± 0.03	75 ± 4	0.684	0.998
	Temkin Isotherm			
	K_T (dm^3 mg^{-1})	b_T (J g mol^{-1} mg^{-1})	χ^2	R^2
VF$_{H2O}$	354 ± 6	242 ± 3	12.247	0.930
VF$_{CO2}$	705 ± 9	243 ± 7	15.829	0.909

Material	Dubinin–Radushkevich Isotherm				
	q_{DR} (mg g^{-1})	K_{DR} (mol^2 J^{-2})	E (J mol^{-1})	χ^2	R^2
VF$_{H2O}$	76.4 ± 0.1	(1.60 ± 0.02) × 10^{-8}	(5.58 ± 0.01) × 10^3	0.497	0.997
VF$_{CO2}$	101 ± 2	(1.41 ± 0.01) × 10^{-8}	(5.95 ± 0.01) × 10^3	0.952	0.995

Material	Sips Isotherm				
	K_s (dm^3 mg^{-1})^{bs}	b_s	q_{max} (mg g^{-1})	χ^2	R^2
VF$_{H2O}$	10.7 ± 0.2	0.917 ± 0.001	80.8 ± 0.1	0.834	0.995
VF$_{CO2}$	8.27 ± 0.03	0.828 ± 0.002	132 ± 3	1.224	0.993

Given that the adsorption energy per mole of adsorbent is <8 kJ mol^{-1}, we can conclude that it is a physisorption process, further supporting the findings based on the analysis of the Sips isotherm. Also, based on Temkin's constant b_T, we can conclude that the adsorption process is exothermic since its values are high and positive [37,38]. Based on the above-presented results and the good fit of the Sips and D-R isotherms, it is likely that the adsorption takes place on the energetically inhomogeneous surface in a combination of mono- and multilayer physisorption.

Linking adsorption kinetics and adsorption thermodynamics to carbon material properties reveals some interesting findings: The fact that the morphology is similar for both used carbons excludes it as a relevant parameter. Moreover, the values of S_{BET} and V_{tot}, which are similar for the two samples, also eliminate them as decisive parameters. In fact, we observe that the kinetics of CHP removal are quite similar, but the VF$_{H2O}$ sample shows slightly higher kinetic constants (Table 2). It cannot be unambiguously claimed that the differences in kinetics are because of the slightly larger pore volume of the VF$_{H2O}$ sample, but it could be a plausible explanation. On the other hand, adsorption thermodynamics differs in terms of adsorption capacities found by Dubinin–Raduskevich and Sips isotherms, suggesting that the VF$_{CO2}$ sample has a higher adsorption capacity than the VF$_{H2O}$ sample. If we recall the results of the EDX analysis, this sample has higher oxygen and phosphorus contents, which likely makes the surface of porous carbon fibers more oxophylic and strongly solvated. In such a scenario, the higher adsorption capacity of the VF$_{CO2}$ sample can be understood on the basis of the combined experimental–theoretical work of Maliyekkal et al. [39]. Using graphene as a model of carbon surface, the authors have demonstrated that pesticide adsorption (including CHP) is mediated by water molecules, which solvate the carbon surface and pesticide molecules, bridging the interactions in that way. It should be noted that CHP can also interact with carbon surfaces with preserved sp^2 domains via aromatic moiety through π-π stacking. However, it is plausible that the interactions via solvent shells could lead to higher adsorption capacities.

3.4. Neurotoxicity of Chlorpyrifos

To assess the neurotoxicity of CHP both before and after treatment with our materials, we followed the procedure outlined in Section 2.3. Our primary objective was to determine if there was an increase in the formation of more toxic compounds when CHP interacted with the adsorbents. This potential increase could result from oxidation, as the thio-forms of organophosphate pesticides may transform into their respective oxo-forms. It is well established that oxo-forms of organophosphate compounds are more potent AChE inhibitors [40].

We tested the highest concentration of CHP investigated in our adsorption measurements (5×10^{-4} mol dm^{-3}). Before treatment, this concentration of CHP inhibited AChE by $90 \pm 3\%$ compared to the control. Following contact with both investigated adsorbents, AChE inhibition was reduced to only $5 \pm 1\%$. The same values of the AChE inhibition for both samples after water treatment and a very small value of the AChE inhibition suggest that the CHP concentration remaining in the solution is shifted to the upper part of the (sigmoidal) AChE inhibition curve (Figure 5), where the inhibition is weakly dependent on the CHP concentration and the differences in adsorption capacities are not reflected in the AChE inhibition. Moreover, these findings suggest that no additional toxic products are formed during adsorption, indicating that all investigated adsorbents can effectively detoxify CHP.
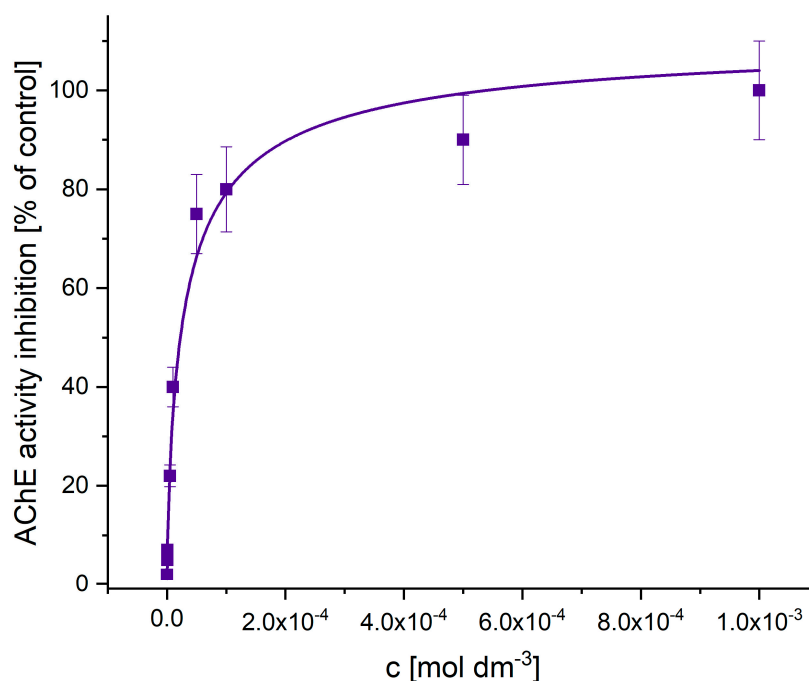

Figure 5. The dependence of AChE (1 U/mL) activity inhibition on CHP concentration. The results are given as a mean value from 3 measurements and expressed as % relative to the control value.

3.5. Where Do We Stand? Comparison with the Literature Data

Considering the detrimental effect of CHP on the human body and ecosystems, it is no surprise that many researchers have become interested in utilizing adsorption for its removal. Table 6 compares CHP adsorption using cellulose fibers with other reported adsorbents. Several studies have investigated different carbonaceous materials derived from agricultural residues, waste products, and synthesized compounds for their CHP adsorption capacities. The Langmuir and Freundlich isotherm models were usually employed to analyze the adsorption data in the reviewed studies, and the former one was used to extract adsorption capacity (as this quantity is not a parameter of the Freundlich equation, see Table 4). The choice of model depended on the nature of the adsorbent and the characteristics of the adsorption process. The Freundlich model, which describes

adsorption on heterogeneous surfaces, was found to fit well in some cases, such as studies involving sugarcane bagasse biochar [41,42], cinnamon stick-derived materials [43], and *Moringa oleifera* seed waste [44]. On the other hand, the Langmuir model, which assumes monolayer adsorption on homogeneous surfaces, was utilized effectively in studies involving polyvinylamine-modified nanocellulose [45], walnut shell biochar [46], and various composite materials [47,48]. Efficiency-wise, the adsorption capacities varied significantly among the different carbon materials tested. For instance, nanocellulose modified with polyvinylamine exhibited a high adsorption capacity of 98.12 mg g^{-1} [45], whereas banana peels, orange peels, pomegranate peels, and date stone-derived carbon materials showed very low capacities ranging from 1.12×10^{-3} to 2.52×10^{-3} mg g^{-1} [49].

Interestingly, some studies explored functionalized carbon materials, such as magnetic graphene oxide, carboxymethyl cellulose, and aminoguanidine-modified magnetic graphene oxide, which demonstrated enhanced adsorption capacities compared to their non-functionalized counterparts. For instance, the adsorption capacity of magnetic graphene oxide and carboxymethyl cellulose was reported as 108.30 mg g^{-1} [50], while aminoguanidine-modified magnetic graphene oxide exhibited a capacity of 85.47 mg g^{-1} [51]. Moreover, the study on functionalized dextrin/graphene oxide composites reported an exceptionally high adsorption capacity of 769.23 mg g^{-1} [47], indicating the potential of such advanced materials for efficient CHP removal. The choice of carbon material significantly influenced the adsorption capacity for CHP, with functionalized and composite materials generally exhibiting higher efficiencies.

Table 6. Comparison of maximum adsorption capacity for CHP removal onto different materials.

Type of Material/Precursor	The Maximum Adsorption Capacity (mg g^{-1})	The Maximum Adsorption Capacity Calculated from	Best Fitting Isotherm Model	Reference
Sugarcane bagasse	3.20	Experimental results	Freundlich	[41]
Sugarcane bagasse-derived biochar	6.25	Experimental results	Freundlich	[42]
Cinnamon sticks	12.37	Langmuir	Langmuir	[43]
Polyvinylamine-modified nanocellulose	98.12	Langmuir		[45]
Moringa oleifera seed waste	25.00	Langmuir	Langmuir, Freundlich	[44]
Activated biochar from tobacco	0.68 using activated biochar 1.60 using chemically activated biochar	Langmuir	Langmuir, Freundlich	[52]
Walnut shell biochar	3.54	Langmuir	Langmuir, Freundlich	[46]
Nano-magnetized and carbonaceous adsorbents obtained from orange peels	68.00, 108.00, and 100.00 for the untreated orange peels, carbonaceous orange peels, and nano-magnetized orange peels	Langmuir	Langmuir, Freundlich	[53]
Nanostructured biochar (nPPAB) was prepared from *Punica granatum* peels	100.00	Langmuir	Langmuir	[54]
Banana peels, orange peels, pomegranate peels and date stones	1.12×10^{-3}, 2.52×10^{-3}, 1.64×10^{-3}, and 1.03×10^{-3} for banana peels, orange peels, pomegranate peels, and date stones			[49]

Table 6. *Cont.*

Type of Material/Precursor	The Maximum Adsorption Capacity (mg g^{-1})	The Maximum Adsorption Capacity Calculated from	Best Fitting Isotherm Model	Reference
Spent coffee grounds	7.00	Langmuir	Langmuir	[16]
Magnetic graphene oxide and carboxymethyl cellulose (MGOC)	108.30	Langmuir		[50]
Aminoguanidine modified magnetic graphene oxide as a robust nanoadsorbent	85.47	Langmuir	Freundlich	[51]
Functionalized dextrin/graphene oxide composite	769.23	Langmuir	Freundlich	[47]
Magnetic chitosan/graphene quantum dot/iron oxide nanocomposite hydrogel beads	39.95	Langmuir	Jossens	[48]
Superhydrophilic graphene oxide/electrospun cellulose nanofibre	3.97	Langmuir	Freundlich	[55]
Graphene-based materials	1.02×10^3 and 2.77×10^3 for industrial-quality graphene and graphene nanoplatelets	Langmuir	Langmuir, Freundlich	[56]
Graphene oxide	98.039	Langmuir	Langmuir	[57]
Cellulose fibers	73 ± 6 (VF$_{H2O}$) 75 ± 4 (VF$_{CO2}$)	Langmuir	Freundlich, Langmuir, and Sips	This study
	80.8 ± 0.1 (VF$_{H2O}$) 132 ± 3 (VF$_{CO2}$)	Sips		

When comparing the q_{max} values from this study obtained from the Langmuir isotherm model, which was most frequently used to extract adsorption capacities (q_{max} values are 73 ± 6 mg g^{-1} and 75 ± 4 mg g^{-1} for VF$_{H2O}$ and VF$_{CO2}$, respectively), with the values from the literature presented in Table 6, it can be seen that the values reported here are comparable with previously published ones. This indicates the high adsorption capacity of the materials used in this study. However, it is essential to consider whether the obtained results are realistic and how justified it is to compare them with literature data, particularly considering non-standardized experimental conditions for accessing adsorption capacities.

The Langmuir model is often used in adsorption studies but is not always entirely realistic. The model assumes monolayer adsorption on a homogeneous surface, which is not always the case in real systems. In many situations, adsorption occurs on more complex surfaces that do not fulfill all the assumptions of the Langmuir model. When comparing the results with values from the literature, caution should be taken due to potential differences in experimental conditions, material characteristics, and analysis methods. For instance, different samples, sample preparations, particle sizes, and experimental conditions can significantly affect adsorption results. Therefore, direct comparison with literature values may be imprecise. Nevertheless, the fact that the q_{max} values from the Langmuir model in this study are comparable with others shown in Table 6 indicates a high adsorption capacity of the investigated porous carbons obtained from cellulose fibers.

4. Conclusions

The presented study highlights the potential of cellulose-based porous carbon fibers as efficient adsorbents for the removal of CHP from water. Physicochemical characterization revealed very high surface areas but similar porosity for both prepared porous carbon fiber samples. Differences could be observed in the chemical composition as the CO$_2$-

activated sample contains more oxygen and, in contrast to the water vapor-activated counterpart, P residues from the DAHP pretreatment. The kinetics of CHP adsorption indicated rapid equilibrium attainment within 10 min, with excellent fitting to the PSO and PFO models. Although CHP adsorption onto VF_{H_2O} materials occurred faster than VF_{CO_2}, both exhibited high initial adsorption rates. The favorable nature of adsorption was supported by a satisfactory fit with both Sips and Dubinin–Radushkevich isotherm models, suggesting a multilayer adsorption process on heterogeneous surfaces. The determined q_{max} values from the Sips isotherm model are 80.8 ± 0.1 mg g^{-1} and 132 ± 3 mg g^{-1} for VF_{H_2O} and VF_{CO_2}, respectively. Higher adsorption capacities for the VF_{CO_2} sample can be explained by solvent-mediated CHP adsorption due to the higher amount of heteroatom functionalities of this carbon. Furthermore, the significant reduction in acetylcholinesterase inhibition following contact with the adsorbents indicates effective detoxification of CHP without the formation of additional toxic by-products. A comparison of the obtained q_{max} values with literature data revealed favorable adsorption capacities of the materials used in this study, indicating their excellent performance. These results suggest that the cellulose-derived porous carbons presented in this study are very efficient CHP adsorbents, making them an attractive material for various applications. Their low cost, availability, and efficiency make them preferable to other materials, such as biomass-derived materials or commercial materials like graphene oxide.

Data Availability Statement: The data used to support the findings of this study can be made available by the corresponding author upon request.

Conflicts of Interest: The authors declare no conflicts of interest.

References

1. Tudi, M.; Yang, L.; Wang, L.; Lv, J.; Gu, L.; Li, H.; Peng, W.; Yu, Q.; Ruan, H.; Li, Q.; et al. Environmental and Human Health Hazards from Chlorpyrifos, Pymetrozine and Avermectin Application in China under a Climate Change Scenario: A Comprehensive Review. *Agriculture* **2023**, *13*, 1683. [CrossRef]
2. Madesh, K.; Chandraleka, R.; Komala, G.; Tripathi, P. *Distribution and Penetration of Insecticides*; P.K. Publishers & Distributors: Ghaziabad, India, 2024; pp. 219–254.
3. Foong, S.Y.; Ma, N.L.; Lam, S.S.; Peng, W.; Low, F.; Lee, B.H.K.; Alstrup, A.K.O.; Sonne, C. A recent global review of hazardous chlorpyrifos pesticide in fruit and vegetables: Prevalence, remediation and actions needed. *J. Hazard. Mater.* **2020**, *400*, 123006. [CrossRef] [PubMed]
4. Rakhimol, K.; Thomas, S.; Volova, T.; Jayachandran, K. *Controlled Release of Pesticides for Sustainable Agriculture*; Springer: Berlin/Heidelberg, Germany, 2020. [CrossRef]
5. EPA United States Environmental Protection Agency. Available online: https://www.epa.gov/ingredients-used-pesticide-products/chlorpyrifos (accessed on 15 April 2024).
6. Wołejko, E.; Łozowicka, B.; Jabłońska-Trypuć, A.; Pietruszyńska, M.; Wydro, U. Chlorpyrifos occurrence and toxicological risk assessment: A review. *Int. J. Environ. Res. Public Health* **2022**, *19*, 12209. [CrossRef] [PubMed]
7. Sud, D.; Kumar, J.; Kaur, P.; Bansal, P. Toxicity, natural and induced degradation of chlorpyrifos. *J. Chil. Chem. Soc.* **2020**, *65*, 4807–4816. [CrossRef]

8. Nandhini, A.R.; Harshiny, M.; Gummadi, S.N. Chlorpyrifos in environment and food: A critical review of detection methods and degradation pathways. *Environ. Sci. Process. Impacts* **2021**, *23*, 1255–1277. [CrossRef]

9. Reigart, J.R. *Recognition and Management of Pesticide Poisonings*; DIANE Publishing: Collingdale, PA, USA, 2009.

10. Marrs, T.C.; Ballantyne, B. *Pesticide Toxicology and International Regulation*; John Wiley & Sons: Hoboken, NJ, USA, 2004.

11. Richardson, R.J. Assessment of the neurotoxic potential of chlorpyrifos relative to other organophosphorus compounds: A critical review of the literature. *J. Toxicol. Environ. Health* **1995**, *44*, 135–165. [CrossRef] [PubMed]

12. Albers, J.W.; Cole, P.; Greenberg, R.S.; Mandel, J.S.; Monson, R.R.; Ross, J.H.; Snodgrass, W.R.; Spurgeon, A.; Van Gemert, M. Analysis of chlorpyrifos exposure and human health: Expert panel report. *J. Toxicol. Environ. Health Part B* **1999**, *2*, 301–324. [CrossRef]

13. U.S. Environmental Protection Agency. *Reregistration Eligibility Science Chapter for Chlorpyrifos, Fate and Environmental Risk Assessment Chapter*; U.S. Environmental Protection Agency: Washington, DC, USA, 2000.

14. Pesticides, O. *Reregistration Eligibility Decision for Chlorpyrifos*; U.S. Environmental Protection Agency: Washington, DC, USA, 2006.

15. Kamrin, M.A. *Pesticide Profiles: Toxicity, Environmental Impact, and Fate*; CRC Press: Boca Raton, FL, USA, 1997. [CrossRef]

16. Milanković, V.; Tasić, T.; Pejčić, M.; Pašti, I.; Lazarević-Pašti, T. Spent Coffee Grounds as an Adsorbent for Malathion and Chlorpyrifos—Kinetics, Thermodynamics, and Eco-Neurotoxicity. *Foods* **2023**, *12*, 2397. [CrossRef] [PubMed]

17. Tasić, T.; Milanković, V.; Batalović, K.; Breitenbach, S.; Unterweger, C.; Fürst, C.; Pašti, I.A.; Lazarević-Pašti, T. Application of Viscose-Based Porous Carbon Fibers in Food Processing—Malathion and Chlorpyrifos Removal. *Foods* **2023**, *12*, 2362. [CrossRef]

18. Vareda, J.P.; Valente, A.J.M.; Durães, L. Assessment of heavy metal pollution from anthropogenic activities and remediation strategies: A review. *J. Environ. Manag.* **2019**, *246*, 101–118. [CrossRef]

19. Soffian, M.S.; Halim, F.Z.A.; Aziz, F.; Rahman, M.A.; Amin, M.A.M.; Chee, D.N.A. Carbon-based material derived from biomass waste for wastewater treatment. *Environ. Adv.* **2022**, *9*, 100259. [CrossRef]

20. Sabzehmeidani, M.M.; Mahnaee, S.; Ghaedi, M.; Heidari, H.; Roy, V.A. Carbon based materials: A review of adsorbents for inorganic and organic compounds. *Mater. Adv.* **2021**, *2*, 598–627. [CrossRef]

21. Aydin, D.; Gübbük, İ.H.; Ersöz, M. Recent advances and applications of nanostructured membranes in water purification. *Turk. J. Chem.* **2024**, *48*, 2. [CrossRef] [PubMed]

22. Jocić, A.; Breitenbach, S.; Bajuk-Bogdanović, D.; Pašti, I.A.; Unterweger, C.; Fürst, C.; Lazarević-Pašti, T. Viscose-Derived Activated Carbons Fibers as Highly Efficient Adsorbents for Dimethoate Removal from Water. *Molecules* **2022**, *27*, 1477. [CrossRef] [PubMed]

23. Gavrilov, N.; Breitenbach, S.; Unterweger, C.; Fürst, C.; Pašti, I.A. Exploring the Impact of DAHP Impregnation on Activated Carbon Fibers for Efficient Charge Storage and Selective O_2 Reduction to Peroxide. *C* **2023**, *9*, 105. [CrossRef]

24. Pérez-Madrigal, M.M.; Edo, M.G.; Alemán, C. Powering the future: Application of cellulose-based materials for supercapacitors. *Green Chem.* **2016**, *18*, 5930–5956. [CrossRef]

25. Liebner, F.; Potthast, A.; Rosenau, T.; Haimer, E.; Wendland, M. Cellulose aerogels: Highly porous, ultra-lightweight materials. *Holzforschung* **2008**, *62*, 129–135. [CrossRef]

26. Magalhães, S.; Fernandes, C.; Pedrosa, J.F.S.; Alves, L.; Medronho, B.; Ferreira, P.J.T.; Rasteiro, M.D.G. Eco-Friendly Methods for Extraction and Modification of Cellulose: An Overview. *Polymers* **2023**, *15*, 3138. [CrossRef] [PubMed]

27. Pandolfo, A.G.; Hollenkamp, A.F. Carbon properties and their role in supercapacitors. *J. Power Sources* **2006**, *157*, 11–27. [CrossRef]

28. Cai, L.-F.; Zhan, J.-M.; Liang, J.; Yang, L.; Yin, J. Structural control of a novel hierarchical porous carbon material and its adsorption properties. *Sci. Rep.* **2022**, *12*, 3118. [CrossRef]

29. Li, W.-K.; Shi, Y.-P. Recent advances of carbon materials on pesticides removal and extraction based determination from polluted water. *TrAC Trends Anal. Chem.* **2024**, *171*, 117534. [CrossRef]

30. Ellman, G.L.; Courtney, K.D.; Andres, V.; Featherstone, R.M. A new and rapid colorimetric determination of acetylcholinesterase activity. *Biochem. Pharmacol.* **1961**, *7*, 88–95. [CrossRef]

31. Lazarević-Pašti, T.D.; Bondžić, A.M.; Pašti, I.A.; Vasić, V.M. Indirect electrochemical oxidation of organophosphorous pesticides for efficient detection via acetylcholinesterase test. *Pestic. Biochem. Physiol.* **2012**, *104*, 236–242. [CrossRef]

32. Breitenbach, S.; Gavrilov, N.; Pašti, I.; Unterweger, C.; Duchoslav, J.; Stifter, D.; Hassel, A.W.; Fürst, C. Biomass-Derived Carbons as Versatile Materials for Energy-Related Applications: Capacitive Properties vs. Oxygen Reduction Reaction Catalysis. *C* **2021**, *7*, 55. [CrossRef]

33. Foo, K.Y.; Hameed, B.H. Insights into the modeling of adsorption isotherm systems. *Chem. Eng. J.* **2010**, *156*, 2–10. [CrossRef]

34. Sips, R. On the Structure of a Catalyst Surface. *J. Chem. Phys.* **1948**, *16*, 490–495. [CrossRef]

35. Kumara, N.T.R.N.; Hamdan, N.; Petra, M.I.; Tennakoon, K.U.; Ekanayake, P. Equilibrium Isotherm Studies of Adsorption of Pigments Extracted from Kuduk-kuduk (*Melastoma malabathricum* L.) Pulp onto TiO_2 Nanoparticles. *J. Chem.* **2014**, *2014*, 468975. [CrossRef]

36. Keren, Y.; Borisover, M.; Bukhanovsky, N. Sorption interactions of organic compounds with soils affected by agricultural olive mill wastewater. *Chemosphere* **2015**, *138*, 462–468. [CrossRef]

37. Mabuza, M.; Premlall, K.; Daramola, M.O. Modelling and thermodynamic properties of pure CO2 and flue gas sorption data on South African coals using Langmuir, Freundlich, Temkin, and extended Langmuir isotherm models. *Int. J. Coal Sci. Technol.* **2022**, *9*, 45. [CrossRef]

38. Smječanin, N.; Bužo, D.; Mašić, E.; Nuhanović, M.; Sulejmanović, J.; Azhar, O.; Sher, F. Algae based green biocomposites for uranium removal from wastewater: Kinetic, equilibrium and thermodynamic studies. *Mater. Chem. Phys.* **2022**, *283*, 125998. [CrossRef]

39. Maliyekkal, S.M.; Sreeprasad, T.S.; Krishnan, D.; Kouser, S.; Mishra, A.K.; Waghmare, U.V.; Pradeep, T. Graphene: A Reusable Substrate for Unprecedented Adsorption of Pesticides. *Small* **2013**, *9*, 273–283. [CrossRef]

40. Colovic, M.B.; Krstic, D.Z.; Lazarevic-Pasti, T.D.; Bondzic, A.M.; Vasic, V.M. Acetylcholinesterase inhibitors: Pharmacology and toxicology. *Curr. Neuropharmacol.* **2013**, *11*, 315–335. [CrossRef]

41. Jacob, M.M.; Ponnuchamy, M.; Kapoor, A.; Sivaraman, P. Bagasse based biochar for the adsorptive removal of chlorpyrifos from contaminated water. *J. Environ. Chem. Eng.* **2020**, *8*, 103904. [CrossRef]

42. Jacob, M.M.; Ponnuchamy, M.; Kapoor, A.; Sivaraman, P. Adsorptive decontamination of organophosphate pesticide chlorpyrifos from aqueous systems using bagasse-derived biochar alginate beads: Thermodynamic, equilibrium, and kinetic studies. *Chem. Eng. Res. Des.* **2022**, *186*, 241–251. [CrossRef]

43. Ettish, M.N.; El-Sayyad, G.S.; Elsayed, M.A.; Abuzalat, O. Preparation and characterization of new adsorbent from Cinnamon waste by physical activation for removal of Chlorpyrifos. *Environ. Chall.* **2021**, *5*, 100208. [CrossRef]

44. Hamadeen, H.M.; Elkhatib, E.A.; Badawy, M.E.I.; Abdelgaleil, S.A.M. Green low cost nanomaterial produced from Moringa oleifera seed waste for enhanced removal of chlorpyrifos from wastewater: Mechanism and sorption studies. *J. Environ. Chem. Eng.* **2021**, *9*, 105376. [CrossRef]

45. Yang, J.; Ma, C.; Tao, J.; Li, J.; Du, K.; Wei, Z.; Chen, C.; Wang, Z.; Zhao, C.; Ma, M. Optimization of polyvinylamine-modified nanocellulose for chlorpyrifos adsorption by central composite design. *Carbohydr. Polym.* **2020**, *245*, 116542. [CrossRef]

46. Tulun, Ş.; Akgül, G.; Alver, A.; Çelebi, H. Adaptive neuro-fuzzy interference system modelling for chlorpyrifos removal with walnut shell biochar. *Arab. J. Chem.* **2021**, *14*, 103443. [CrossRef]

47. Hassanzadeh-Afruzi, F.; Esmailzadeh, F.; Taheri-Ledari, R.; Maleki, A. High adsorption capability of chlorpyrifos and Congo red in aqueous samples by a functionalized dextrin/graphene oxide composite. *Int. J. Environ. Sci. Technol.* **2023**, *20*, 10731–10750. [CrossRef]

48. Barzegarzadeh, M.; Amini-Fazl, M.S.; Sohrabi, N. Ultrasound-assisted adsorption of chlorpyrifos from aqueous solutions using magnetic chitosan/graphene quantum dot-iron oxide nanocomposite hydrogel beads in batch adsorption column and fixed bed. *Int. J. Biol. Macromol.* **2023**, *242*, 124587. [CrossRef]

49. Hussain, O.A.; Hathout, A.S.; Abdel-Mobdy, Y.E.; Rashed, M.M.; Abdel Rahim, E.A.; Fouzy, A.S.M. Preparation and characterization of activated carbon from agricultural wastes and their ability to remove chlorpyrifos from water. *Toxicol. Rep.* **2023**, *10*, 146–154. [CrossRef]

50. Dolatabadi, M.; Naidu, H.; Ahmadzadeh, S. Adsorption characteristics in the removal of chlorpyrifos from groundwater using magnetic graphene oxide and carboxy methyl cellulose composite. *Sep. Purif. Technol.* **2022**, *300*, 121919. [CrossRef]

51. Mahdavi, V.; Taghadosi, F.; Dashtestani, F.; Bahadorikhalili, S.; Farimani, M.M.; Ma'mani, L.; Mousavi Khaneghah, A. Aminoguanidine modified magnetic graphene oxide as a robust nanoadsorbent for efficient removal and extraction of chlorpyrifos residue from water. *J. Environ. Chem. Eng.* **2021**, *9*, 106117. [CrossRef]

52. Celso Gonçalves, A.; Zimmermann, J.; Schwantes, D.; Tarley, C.R.T.; Conradi Junior, E.; Henrique Dias de Oliveira, V.; Campagnolo, M.A.; Ziemer, G.L. Renewable Eco-Friendly Activated Biochar from Tobacco: Kinetic, Equilibrium and Thermodynamics Studies for Chlorpyrifos Removal. *Sep. Sci. Technol.* **2022**, *57*, 159–179. [CrossRef]

53. Asghar, A.; Mabarak, S.; Ashraf, B.; Rizwan, M.; Massey, S.; Asghar, B.H.; Shahid, B.; Rasheed, T. A sustainable approach for the removal of chlorpyrifos pesticide from aqueous phase using novel nano magnetized biochar. *Inorg. Chem. Commun.* **2024**, *159*, 111790. [CrossRef]

54. Hamadeen, H.M.; Elkhatib, E.A. Nanostructured modified biochar for effective elimination of chlorpyrifos from wastewater: Enhancement, mechanisms and performance. *J. Water Process Eng.* **2022**, *47*, 102703. [CrossRef]

55. Aris, N.I.F.; Rahman, N.A.; Wahid, M.H.; Yahaya, N.; Abdul Keyon, A.S.; Kamaruzaman, S. Superhydrophilic graphene oxide/electrospun cellulose nanofibre for efficient adsorption of organophosphorus pesticides from environmental samples. *R. Soc. Open Sci.* **2020**, *7*, 192050. [CrossRef]

56. Lazarević-Pašti, T.; Anićijević, V.; Baljozović, M.; Anićijević, D.V.; Gutić, S.; Vasić, V.; Skorodumova, N.V.; Pašti, I.A. The impact of the structure of graphene-based materials on the removal of organophosphorus pesticides from water. *Environ. Sci. Nano* **2018**, *5*, 1482–1494. [CrossRef]

57. Yadav, S.; Goel, N.; Kumar, V.; Singhal, S. Graphene Oxide as Proficient Adsorbent for the Removal of Harmful Pesticides: Comprehensive Experimental Cum DFT Investigations. *Anal. Chem. Lett.* **2019**, *9*, 291–310. [CrossRef]